Contrib. Mineral. Petrol. 74, 123–133 (1980)

Contributions to Mineralogy and Petrology

The Orthoclase-Microcline Inversion: A High-Resolution Transmission Electron Microscope Study and Strain Analysis

Richard A. Eggleton[1] and Peter R. Buseck[2]

[1] Geology Department, Australian National University, Canberra, ACT 2600, Australia
[2] Departments of Chemistry and Geology, Arizona State University, Tempe AZ, USA

Abstract. High-resolution electron microscopy of an intermediate microcline (Or_{93}) from a granodiorite in southeastern Australia reveals an *en echelon* arrangement of triclinic lens-shaped domains, twinned on the albite law. The domains are tabular on (010), are only a few unit cells wide, but extend 20 or 30 unit cells along x, until they merge into a zone of monoclinic cells roughly aligned in the rhombic section. The domains are longer and less clearly terminated along z. Strain calculations show that the energy released by Al/Si ordering, producing the orthoclase-microcline inversion, is equal to the strain energy developed when triclinic domains are forced to retain the original monoclinic crystal shape. This balance of strain energies thus explains the metastable persistence of intermediate microcline into the region of maximum microcline stability. Shearing along faults during deformation of the granodiorite released the strain in some of these feldspars, allowing maximum microcline to develop, and so giving rise to a bimodal distribution of triclinicities throughout the pluton. The value of γ measured for the intermediate microcline is the average of a range of values throughout each domain, and may be considerably closer to 90° than γ from an unstrained crystal with the same degree of Al/Si order.

Introduction

High sanidine displays total Al/Si disorder, whereas low microcline is completely ordered; they are end members of a well recognized continuum of structural states in K-feldspars. The words "high" and "low" refer, at least implicitly, to the temperature at which the feldspar crystallized, and for volcanic sanidine and authigenic microcline the correlation is evidently sound. Plutonic K-feldspar crystallizes at high temperature, cools to some lower temperature while maintaining structural equilibrium, and then cools further in apparent disequilibrium, retaining the partially ordered orthoclase structure. When orthoclase does change to microcline, both pericline and albite twins develop because the crystal is forced to occupy a fixed shape while changing geometry (Goldsmith and Laves 1954). Optical microscopy has shown that such inverted microclines are a complex of domains, but the technique cannot resolve the details of the resulting texture.

The metastable persistence of orthoclase into the stability field of maximum microcline places a severe restriction on the use of Al/Si distribution to interpret the conditions of crystallization of the feldspar. The inversion to microcline is influenced by a variety of physical and chemical factors. Martin (1974), in summarizing them, considers temperature, time, pressure, deformation, and surface area as physical controls on ordering; and the presence of an aqueous phase, the K:Na:Ca proportions of the feldspar, and the bulk rock composition as chemical controls. Because the structure of the domains in microcline has not been completely described, the relative importance of the foregoing factors is unknown, and so it has been impossible to interpret the final stages of feldspar crystallization. We will show that the energy released when orthoclase orders toward microcline is insufficient to overcome the strain produced when the triclinic lattice is forced to conform to a monoclinic crystal shape.

During the cooling of a plutonic K-feldspar, the Al progressively concentrates in the tetrahedral site designated $T_1(0)$ (Megaw 1956), and the manner of its migration within the crystal has been termed the "ordering path" (Stewart and Ribbe 1969). Attempts

Reprint requests to: R.A. Eggleton

0010-7999/80/0074/0123/$02.20

to define the ordering path have been based on observed variations in cell geometry and optics during the transition from high sanidine to maximum low microcline. Such changes have been used to develop the concept of a smooth variation of property with order, allowing the structural state of unknown samples to be deduced from physical properties alone (e.g., Wright and Stewart 1968). There are three widely used parameters for defining the degree of Al/Si order in a particular K-feldspar. The "triclinicity" of Goldsmith and Laves (1954) and the triclinic indicator $\Delta\alpha^*\gamma^*$ of Stewart and Ribbe (1969), range from zero in monoclinic feldspars to one in low albite and maximum microcline. The Δbc order indicator of Stewart and Ribbe (1969), ranges from 0.5 in disordered feldspars to 1.0 in fully ordered feldspars.

Variation in ordering path can be useful for interpreting the crystallization history of a suite of feldspars (Smith 1974; Stewart and Wright 1974). Eggleton (1979) showed that a suite of igneous K-feldspar megacrysts from the Kameruka granodiorite in southeastern Australia had ordered from orthoclase to microcline during shearing. In the bulk of the pluton, the feldspar is either orthoclase (based on Guinier Camera measurements) or intermediate microcline of small triclinicity (<0.2). However, along faults it has been converted to maximum microcline (triclinicity = 1). On the basis of a $\Delta bc - \Delta\alpha^*\gamma^*$ plot, these inverted feldspars have a bimodal triclinic population. Individuals from each group define an ordering path parallel to the ordering path of albite (Fig. 1), but with a discontinuity between the two parallel segments.

X-ray measurements, although able to define ordering paths, do not reveal the reason for variations between suites of feldspars, nor, for example, explain the discontinuity in the Kameruka data. We have used the methods of high-resolution transmission electron microscopy (HRTEM) to examine the inversion process in detail. By investigating a domain structured intermediate microcline from a feldspar suite for which the ordering path has been determined, the features observed in the HRTEM images can be used to interpret aspects of the inversion mechanism.

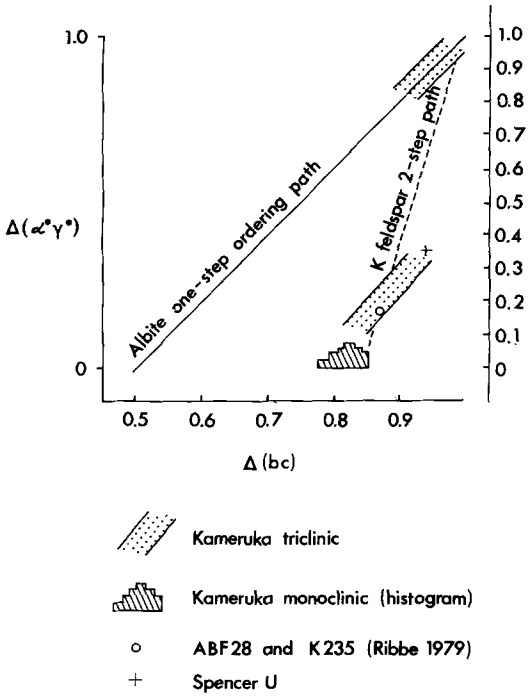

Fig. 1. Δbc *vs* $\Delta\alpha^*\gamma^*$ for various alkali feldspar ordering paths, following Smith (1974). The Kameruka path has a lower slope than the bulk of samples reported in the literature, and moreover shows a marked discontinuity in $\Delta\alpha^*\gamma^*$

Sample and Methods

For this study we selected sample ABF 28 of Eggleton's 1979 Kameruka suite. It is from the Brogo dam site, where there have been extensive excavations, and it is thus one of the best exposed localities in this pluton. Aerial photographs show a pronounced lineament trending NNW along Brogo Creek, comparable to many such lineaments in the area. The lineaments are related to parallel basic dykes that cut the granites of the Bega Batholith. There is, however, no field evidence for faulting in this locality.

The sample is an intermediate microcline, $a=8.579$ Å, $b=12.973$ Å, $c=7.205$ Å, $\alpha=90.08°$, $\beta=115.99°$, $\gamma=89.58°$, $\Delta bc=0.87$, $\Delta\alpha^*\gamma^*=0.16$; composition $Or_{93}Ab_7$. On the basis of the feldspar order indicators, the sample has the same degree of order as does K235, an intermediate microcline for which Ribbe (1979) has determined the crystal structure. Three different megacrysts from the Brogo locality were examined using a JEOL JEM 100B transmission electron microscope. The earlier work on these feldspars has shown that structural state and composition are constant over a single sample locality; TEM showed features that are similar in each of the megacrysts. Samples were prepared by thin-sectioning, followed by ion-beam milling using the same procedures as described by Veblen and Buseck (1979).

The identity of the feldspar in each section was determined after calibrating the d-spacings observed with the electron microscope by using a gold-coated ion-thinned feldspar crystal, and then by tilting experiments with the actual samples to confirm crystallographic orientations. The greatest risk of misidentification is that albite might be confused with K-feldspar. However, for the three main crystallographic projections used there are diagnostic parameters that allow ready distinction between Na- and K-feldspars: d_{201}/d_{020} for [102], d_{200}/d_{020} for [001], and α for [100]. For each sample we used the diffraction patterns to identify and orient the crystals, but we have used lattice fringe imaging to study the inversion process.

High Resolution Transmission Electron Microscopy

Three distinctive types of regions, designated "uniform-", "dimpled-", and "coarsely twinned terrane"

can be seen in electron micrographs of this feldspar. Uniform terrane is untwinned and, within experimental error, monoclinic (Fig. 2). While not difficult to find, uniform terrane is not common. Dimpled terrane contains evident regions of different contrast that represent distinct crystallographic domains. It is shown in Figs. 2–5 and as a diagram in Fig. 6. Coarsely twinned terrane (Fig. 5) is not common; it shows uniformly spaced (010) twin planes separating featureless (and thus unstrained) lamellae. The ends of the lamellae grade into dimpled terrane, with a marked change in lattice orientation, as revealed by changes in contrast.

From their cell dimensions, we interpret uniform terrane as orthoclase and coarsely twinned terrane as maximum microcline. We interpret dimpled terrane as showing a checkerboard pattern of right- and left-handed albite-twinned domains, tabular on (010). The (010) twin planes between domains are not perfectly straight; commonly there is a shift sideways of one or two lattice fringes from one domain to the next. The domains range in size; some representative measurements of length and width from different crystals are listed in Table 1. *hOl* lattice fringes crossing (010) are detectably non-orthogonal, but the angles are much closer to 90° than those in coarsely twinned terrane; hence we regard dimpled terrane as intermediate microcline. Sample ABF 28 therefore shows three stages in the ordering of the Kameruka K-feldspars; residual orthoclase, dominant intermediate microcline and minor maximum microcline. In the following sections we analyse the ordering path more fully.

Strain During Inversion

Evaluation of the build-up of strain associated with the change from monoclinic to triclinic geometry has been an integral part of all discussions of the orthoclase-microcline inversion. Goldsmith and Laves (1954) observed that: "Normally monoclinic material may be forced to be triclinic, and vice-versa", and McConnell (1971) detected two sets of orthogonal distortion waves producing domains in adularia. Smith (1974) refers repeatedly to strain effects in intermediate microclines, concluding (p. 73) "... a domain texture is so common for K-feldspars from igneous rocks that it either represents a trend of quenched equilibrium or a highly metastable situation". Dimpled terrane appears to be a configuration that allows a lattice of low triclinicity to accommodate to an original monoclinic shape without breaking Si–O bonds and without introducing defects. Instead, the lattice undergoes strain, particularly where domains of opposite hand join, so that the change of hand is gradual rather than discontinuous.

Changes in the orientation of the feldspar lattice from one domain to the next are especially clear in [102] projection. The single wedge-shaped row of domains in Fig. 2a represents the start of the development of dimpled terrane from the surrounding uniform terrane. The angle (010): $(\bar{2}01)$ varies sinusoidally between domains, from maximum obliquity at the domain center to orthogonal at domain boundaries. We refer to such a lattice variation and domain type as "sinusoidal".

Maximum microcline lamellae in coarsely twinned terrane are shown in Fig. 5. The crystal appears free of strain and displays straight $(\bar{2}01)$ lattice planes. Across the (010) twin boundary these planes define a chevron pattern; where such a character appears in intermediate microcline we refer to "chevron domains".

Extensive dimpled terrane is not as easily interpreted as the previous examples, because lattice resolution is lost at many domain boundaries as a result of orientation changes in the plane of projection. Viewing Fig. 4a at low angle along y reveals a sinusoidal pattern to $(\bar{2}01)$, but with a smaller amplitude than in Fig. 2b, as well as an indication of an abrupt, chevron-like angular change at (010) domain boundaries. Dimpled terrane is probably composed of domains having part chevron, part sinusoidal character.

The nature of the domain boundaries parallel to y is even less clear. Electron diffraction patterns only reveal albite twin orientations, with streaking parallel to y; there is no diffraction evidence for pericline twinning. McLaren (1978) discusses the evidence for combined albite-pericline twinning in microcline, and concludes that the two twin types occur in separate areas of crystal. McLaren suggests that the pericline twins degrade, leaving domains in albite-twin relationship, but with varying degrees of misorientation between them. Images of dimpled terrane show no sharp boundaries that correspond to the pericline twin plane; instead, lens-shaped domains of alternate hand (albite law) interfinger. We interpret the geometrical relation as in Fig. 6, in which the left- and right-handed domains have part chevron, part sinusoidal character. Between the "tips" of the lenses are monoclinic diamond-shaped domains, possibly aligned along the pericline plane. For the purpose of later strain analysis, this model will be simplified by reintroducing the pericline plane as a single surface in order to describe orthogonal domains. However, we doubt whether such a planar surface exists; rather, we postulate a broad zone of dominantly monoclinic

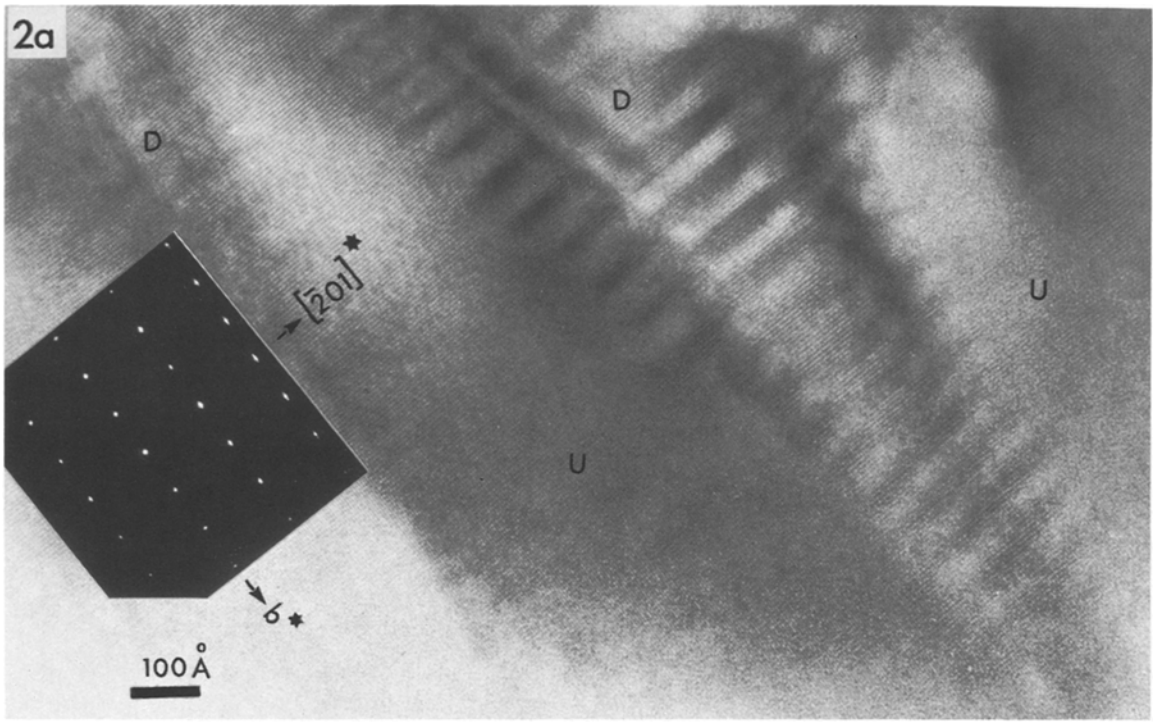

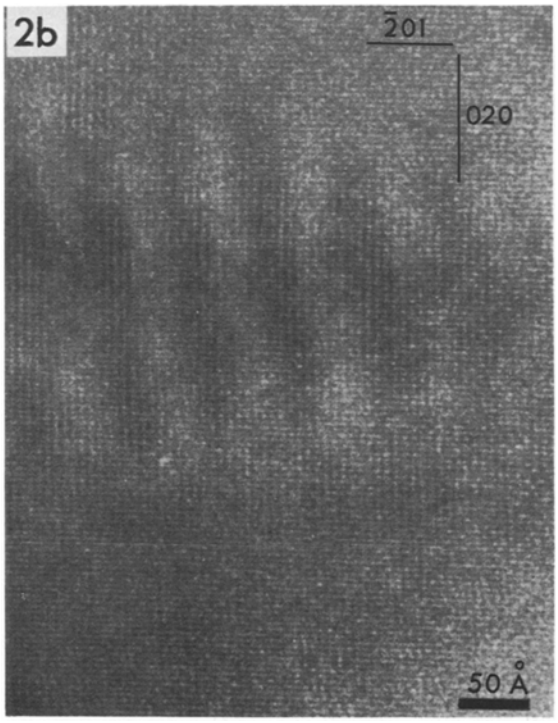

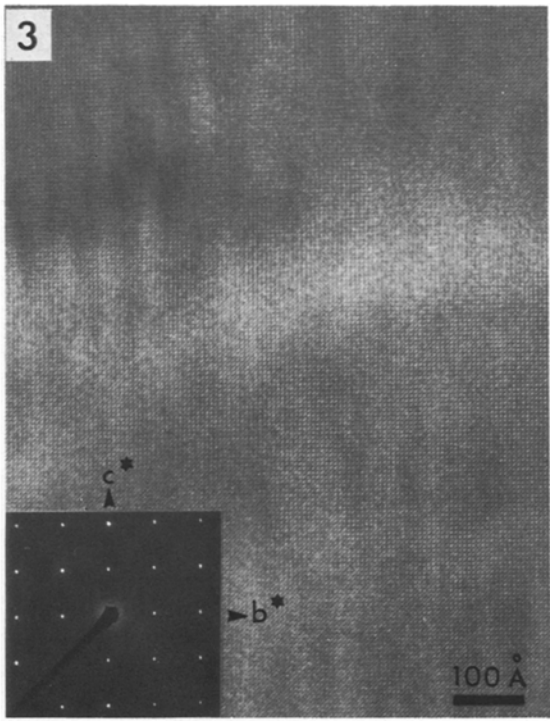

Fig. 2a and b. Types of feldspar terranes as observed by HRTEM. **a** Uniform terrane (*U*) with wedges of dimpled terrane (*D*); [102] projection. **b** Enlargement of part of **a**, showing sinusoidal ($\bar{2}$01) lattice planes in dimpled terrane. Best seen by viewing along ($\bar{2}$01)

Fig. 3. HRTEM image of dimpled terrane; [100] projection

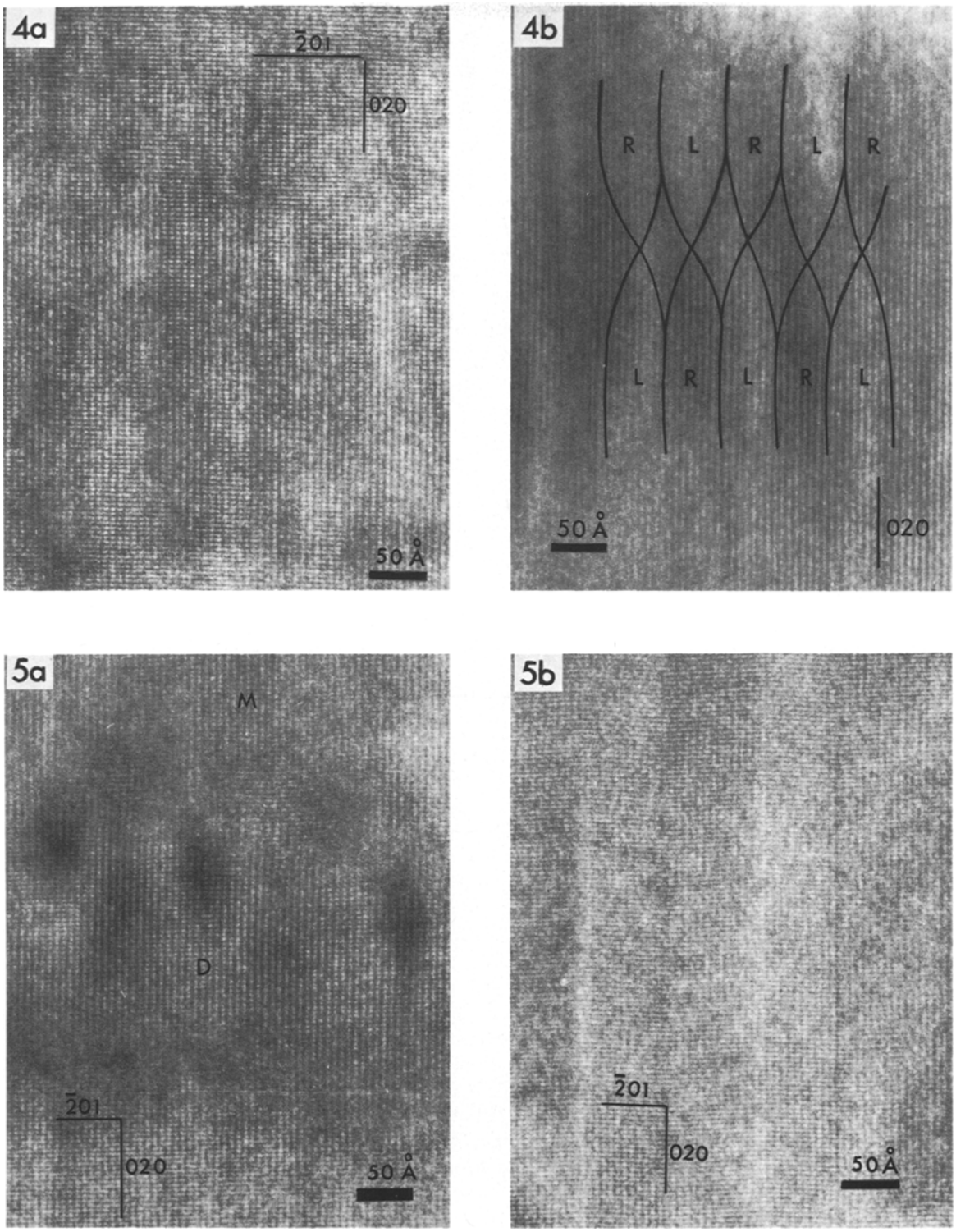

Fig. 4a and b. HRTEM images of dimpled, domain textured terrane; [102] projection. Some domain boundaries are indicated; the domains are arbitrarily labelled *L* (*left handed*) and *R* (*right handed*). **a** Shows mixed sinusoidal and chevron character to the ($\bar{2}$01) planes and straight (020) lattice planes. **b** Slightly misoriented, showing (020) lattice planes and clearer *en echelon* arrangement of the lens-shaped domains

Fig. 5a and b. HRTEM image of dimpled and coarsely twinned terrane; [102] projection. **a** Maximum microcline with albite twinning, (*M*) grading into dimpled terrane, (*D*). **b** Adjacent region to **a**, showing chevron pattern of ($\bar{2}$01) lattice planes in unstrained maximum microcline

Table 1. Domain dimensions

L	M	N	M/L
16	2		0.12
20	2.5[a]		0.12
25	3		0.12
30	3		0.10
35	3.5[a]		0.10
	2	80	
	2.5[a]	50	
	4	150	

L=number of unit cells //x; M=number of unit cells //y; N=number of unit cells //z^*

[a] domain with an odd number of 020 fringes

Table 2. Summary of HRTEM observations and ordering data for Kameruka K-Feldspars

Mineral	HRTEM observations		Ordering estimators		Γ[a]
	Terrane type	Domain type	$\Delta\alpha^*\gamma^*$	Δbc	
Orthoclase	Uniform	None	0	0.5–0.85	0
Intermediate microcline	Dimpled	Sinusoidal	0.2–0.4	0.85–0.95	~0.01
Maximum microcline	Coarsely twinned	Chevron	1.0	1.0	0.04

[a] $\Gamma=\frac{(90-\gamma)\pi}{180}$

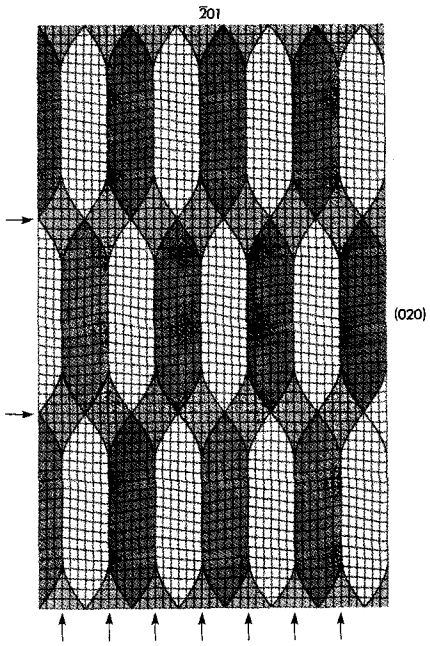

Fig. 6. Diagrammatic representation of (020) and ($\bar{2}$01) lattice planes in dimpled terrane. The figure shows domains with part chevron, part sinusoidal variation in obliquity, arranged en echelon. Left-hand domains are *shaded darkest*, monoclinic regions *lighter*, and right-hand domains are *unshaded*. Domain bounding surfaces are *arrowed*. (Half the ($\bar{2}$01) planes are omitted for clarity)

cells parallel to the rhombic section, separating wider strips of triclinic, albite-twin related, *en echelon* domains.

Projections along [100] (Fig. 3) reveal a terrane that is qualitatively similar to the dimpled terrane of [102] projection (Fig. 2). Because α^* in microcline is so close to 90°, no assessment can be made of the variation of the (001) lattice plane orientation across (010). For such a slight deviation from 90°, the difference between sinusoidal and chevron character is small enough to be negligible in this analysis.

X-Ray Diffraction From Domains

The X-ray patterns from sinusoidal, chevron, and mixed domains can be expected to show differences for paired, γ-sensitive reflections such as 131, $1\bar{3}1$. A domain can be characterized by the distribution of γ over its volume, specifically in the form of a graph showing the number of unit cells having a particular value of γ (using the simplifying assumption of rigid cells with small angular changes between them). Figure 7 shows diagrams for sinusoidal, chevron, and mixed domains.

Sinusoidal domains have only the central cell with maximum obliquity, and a large number of cells with zero obliquity (at all domain boundaries). Between these extremes there is a roughly inverse linear relation between degree of obliquity and the number of unit cells having that obliquity. The 131 reflection from a sinusoidal domain should show a single peak with intensity maximum at the monoclinic position (the greatest number of cells have a monoclinic shape), but broader than a true monoclinic reflection.

A given chevron domain has equal numbers of cells for all values of γ between 90° and maximum obliquity, because γ is constant for a row of cells parallel to y. In this case X-ray patterns should show a broad flat-topped 131 peak, again centred on the monoclinic position, indicating the presence of triclinic character (Smith 1974; Fig. 7:30, e).

Mixed domains have their central cell with maximum obliquity, but only a few end cells are monoclinic. The most abundant obliquity is that at the (010) domain boundaries along the central row of the domain parallel to y. The predicted X-ray pattern would have distinct 131 and $1\bar{3}1$ reflections with a diffuse region between them (Smith 1974; Fig. 7:30b).

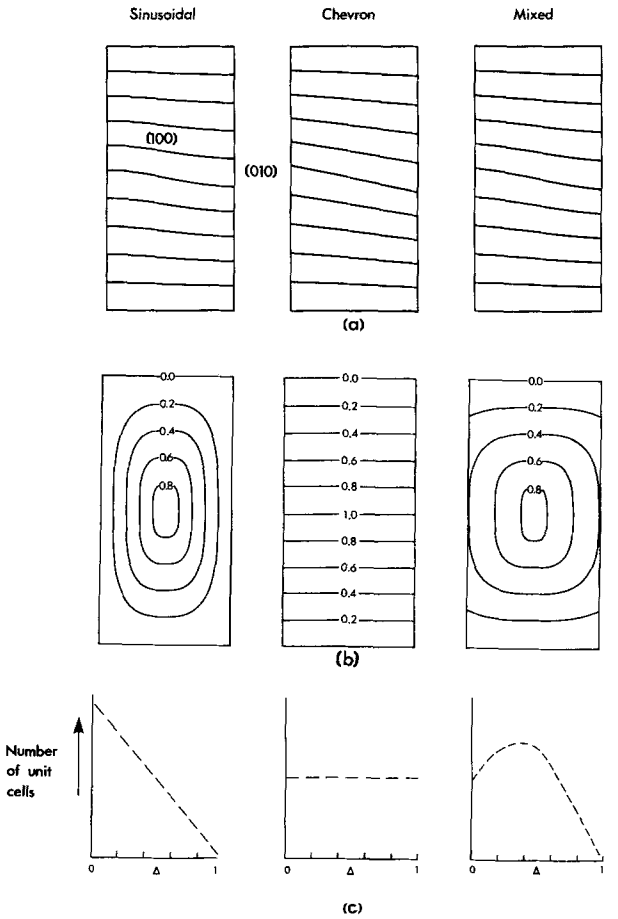

Fig. 7. a Diagrams of ideal sinusoidal, mixed, and chevron domains in microcline constrained to monoclinic domain shape. **b** Schematic diagram of contours of obliquity (monoclinic $\Delta = 0$, maximum triclinic $\Delta = 1.0$) for sinusoidal, chevron, and mixed domains. Each sketch corresponds to the distribution of Δ within a single domain. **c** Frequency plot showing the numbers of unit cells having a given obliquity. The 131 X-ray reflection profile is dictated by these trends

Domain Formation

The development of domain texture results from a balance between elastic and twin energies. Chevron domains have roughly half the elastic strain of sinusoidal domains (see below), but at each (010) boundary there is a lattice energy increase because of twinning. Sinusoidal domains have monoclinic cells on either side of the (010) domain (twin) boundary and so have little or no twin-plane energy increase, since no adjacent cells are in albite twin relation.

Combining the X-ray and electron-optical observations, we conclude that at $\Delta bc \simeq 0.8$ orthoclase, with equal content of Al in T_1 (o) and T_1 (m), begins to adopt triclinic character. At first sinusoidal domains form, and the crystals remain monoclinic to X-ray measurements. At $\Delta bc = 0.85$, the energy balance between elastic strains and twinning dictates the formation of some chevron character in the domains, they become mixed (Fig. 7b), and discrete triclinic reflections appear on the X-ray patterns (the situation for the bulk of ABF28). At this stage the measured triclinity, as determined by X-ray methods, would be that of the largest number of cells (e.g., the "mixed" domain of Fig. 7), and "would be considerably less than would be expected from the degree of order present" (Goldsmith and Laves 1954); as Smith (1974, p. 267) says: "domain texture causes the angles to be constrained towards monoclinic values". Such a crystal, for example, might have an Al/Si distribution that theoretically should produce an obliquity ($\Delta\alpha^*\gamma^*$) of e.g., 0.8 but because of the strain, the most abundant obliquity would be much less, e.g., 0.3.

If the order parameter, Δbc, is unaffected by strain (and its continuity, (Fig. 1) in contrast to the discontinuity in $\Delta\alpha^*\gamma^*$, suggests this as a reasonable assumption), then the slope of the Δbc *vs* $\Delta\alpha^*\gamma^*$ graph for a strained crystal would be flattened relative to an unstrained crystal. The slope for the Kameruka feldspars between $\Delta bc = 0.85$ and 0.9 (Fig. 1) exactly bears out this prediction. Conceivably, ordering could go to completion ($\Delta bc = 1.0$) while the cell angles remained constrained to intermediate triclinicity values, but this extreme is not evident in the Kameruka data.

Strain Energy, Es

Upon cooling, internal energy is released from the crystal by Al/Si ordering. However, strain energy is simultaneously generated by the changes in geometry that are produced during the tendency for the crystal to invert from monoclinic to triclinic symmetry and structure. In order to evaluate these opposing effects we have calculated both the strain energy and the inversion (or ordering) energy. The electron microscope observations provide necessary geometrical input for the former, whereas the latter is based on thermodynamic and X-ray data.

Analysis of elastic strain is presented here for sinusoidal domains, as these have no complicating twin-boundary configuration and thus no associated twinning energies. (Calculations for chevron domains have also been made, and yield a strain energy about half that found for sinusoidal domains of equal size.) The essential features of the model are:

1. A three-dimensional "checkerboard" of domains form, alternately in left- and right-hand albite twin orientation, tabular on (010);

2. The domains are bounded by an (010) surface, by the pericline twin plane, and by an (001) surface;

3. (010) lattice planes are undistorted, all atomic movement resulting from changes in α and γ occurs parallel to (010);

4. Changes in b and d_{001} are negligible compared to the angle-compensating movements;

5. Domain boundaries remain stationary as inversion proceeds, allowing strain analysis of each domain independent of its neighbours;

6. Domain boundaries are orthogonal (the pericline twin plane is actually at 84° to (001) in maximum microcline);

7. Unit cells at the domain centre have α and $\gamma \neq 90°$, cells at the domain edges are monoclinic; between these extremes, α and γ vary sinusoidally (Fig. 6).

The smallest observed domains contain more than 2,000 unit cells, ($>16\times2\times50$, Table 1). We assume that when some cells have ordered to the maximum microcline distribution of Al/Si and others have not, the strain is distributed in the same way as if all cells had equally, but partly, ordered (this is the same assumption that is used for X-ray structure analysis of intermediate microcline).

To describe the degree of order, or triclinicity, we use the γ-cell angle, which in Kameruka maximum microcline is 87.67°. The function $(90-\gamma)$, expressed as radians, proves to be more convenient than γ. We define $\Gamma=\pi\ (90-\gamma)/180$ as the triclinic indicator for this analysis. The cell angle α reaches 90.6 in maximum microcline, or one quarter the departure from 90° reached by γ. We assume a constant ratio of $(90-\gamma)/(\alpha-90)$ of 4 (the average ratio for 20 Kameruka microclines is 3.5).

Figure 8 shows part of an idealized microcline domain, L unit cells $//x,M//y,N//z$, viewed along (001). The reference orthogonal axes OX, OY, OZ, parallel x, y, and z^* respectively. The point (0,0,0) is at the domain center.

For the analysis of infinitesimal strains (Nye, 1972), the displacement that every point in an elastic body undergoes as the result of an applied stress must be defined. For our model, we consider a triclinic domain which has been constrained to occupy a monoclinic shape in such a way that all the displacement is parallel to (010) (i.e., the y coordinate of each point is unchanging), and in addition, points along the axes OX, OZ, are unmoved. In the unstrained crystal, x', and z' can be stated in terms of y and γ relative to orthogonal axes, as $x'=x+y\Gamma$, $z'=z+y\Gamma/4$; where x, z, are the coordinates of the lattice row passing through x', y, z' at $y=0$ (Fig. 8).

Under the influence of stress each point x', y, z' is displaced to new coordinates x'', y, z'', and according to the model, this displacement is sinusoidal in character for lattice rows along OY, being a maximum at domain boundaries. The wavelength of the displacement is equal to 2 domain widths parallel to OY and 2 domain lengths parallel to OZ (Fig. 6). Because α is very small, the difference between a sinusoidal and a linear displacement parallel to OZ is negligible, and a simpler linear model is used here.

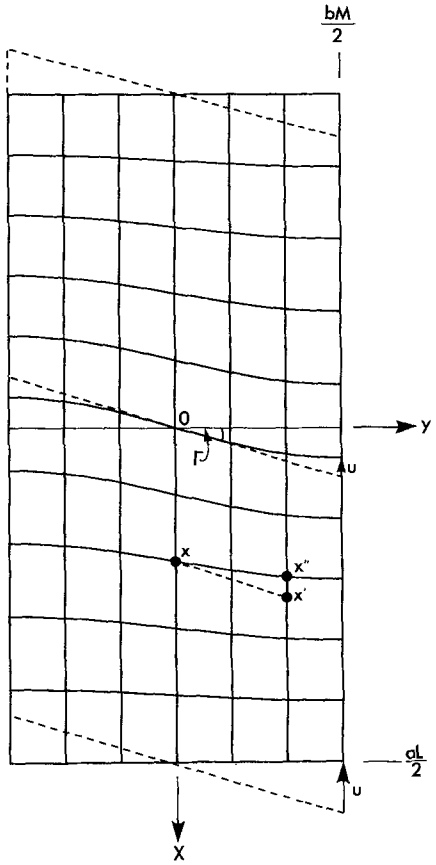

Fig. 8. Diagrammatic representation of a sinusoidal domain. The *broken line* represents the unstrained domain shape. Strain produces the lattice displacement, u, parallel to x; it is indicated at $(0, bM/2)$ and $(aL/2, bM/2)$. The angle is greatly exaggerated for clarity

The problem is thus reduced to the analytical description of lattice rows of sinusoidal shape along OY, whose amplitude decreases in directions away from OY. The periodic function describing each lattice row is determined by its slope (Γ') at $y=0$, a slope which ranges from Γ at the domain centre (0,0,0), to zero at the domain ends $\left(\text{e.g. } \frac{aL}{2}, 0, 0\right)$ assuming the variation of slope to be linear in x, $\Gamma' = \left(1-\frac{2x}{aL}\right)\Gamma$. We can thus express x'', the x-coordinate of any point in the stressed crystal, in terms of a lattice row coordinate at $y=0$ (constant under the

stress described here), the slope of the lattice row (Γ) at this point, and the wave length ($=2bM$),

$$x'' = \left(1-\frac{2x}{aL}\right)\frac{bM\Gamma}{\pi}\sin\left(\frac{\pi Y}{bM}\right).$$

The difference in x between the strained and unstrained lattice is thus

$$u = x' - x'' = y\Gamma - \left(1-\frac{2x}{aL}\right)\frac{bM\Gamma}{\pi}\sin\frac{\pi y}{bM}.$$

For the displacement $w(=z'-z'')$ we only require a function that is 0 at $y=0$ and $z=0$ and which reaches a maximum of $w=\frac{bM}{2}\tan(90-\alpha)$ at $\left(x, \frac{bM}{2}, \frac{cN}{2}\right)$ (i.e., the four corners of the triclinic domain in [100] projection are pushed into rectangular shape, as in a chevron domain (Fig. 7a)). The electron micrographs do not show the nature of the lattice distortion in this projection, and the linear function is the simplest. We therefore arrive at: $w = yz\frac{\Gamma}{4}\frac{2}{cN}$ $\left(\text{remembering that } (\alpha-90)\sim\frac{\Gamma}{4}\frac{180}{\pi}\right)$.

Using these expressions for the displacements (u, v, w) of a point (x, y, z), the strain matrix, e_i, can be formed from the partial derivatives

$$\frac{\partial u}{\partial x}, \frac{\partial u}{\partial y}, \frac{\partial u}{\partial z}, \frac{\partial v}{\partial x}, \text{ etc.}$$

$$e_i = \begin{vmatrix} \frac{2bM}{\pi aL}\Gamma\sin\left(\frac{\pi y}{bM}\right) \\ 0 \\ y\Gamma/2cN \\ z\Gamma/2cN \\ 0 \\ \Gamma-\left(1-\frac{2x}{aL}\right)\Gamma\cos\left(\frac{\pi y}{bM}\right) \end{vmatrix}.$$

For a small volume $\Delta V(=\Delta X\,\Delta Y\,\Delta Z)$, the strain energy $E_s=\frac{1}{2}C_{ij}e_ie_j\,\Delta X\,\Delta Y\,\Delta Z$ Joule, where the C_{ij} values are the elastic stiffness constants in N/m^2. The total strain energy of the domain is therefore

$$E_s = 8\int_0^{\frac{aL}{2}}\int_0^{\frac{bM}{2}}\int_0^{\frac{cN}{2}}\tfrac{1}{2}C_{ij}e_ie_j\,\partial x\,\partial y\,\partial z,$$

assuming the eight octants have the same strain energy.

This triple integral is:

$$E_s = \frac{abcLMN}{2}\Gamma^2\left[\frac{2C_{11}}{\pi}\frac{b^2}{a^2}\frac{M^2}{L^2}+\frac{C_{13}b^2M^2}{\pi^3acLN}+\frac{C_{33}b^2M^2}{48c^2N^2}+\frac{C_{44}}{48}+\frac{C_{46}(1-1/\pi)}{4}+C_{66}\left(\frac{4}{3}-\frac{2}{\pi}\right)\right].$$

For the C_{ij} values we used the average of those given by Ryzhova et al. (1965) for orthoclase and microcline. Although their values are for less potassic compositions than the Kameruka samples, their data indicate a relatively narrow range for the elastic properties of feldspar. Evaluation of the constants leads to a strain energy per unit cell:

$$E_s = \Gamma^2\left(10\frac{M^2}{L^2}+1.2\frac{M^2}{LN}+3\frac{M^2}{N^2}+8.8\right)\times10^{-18}J.$$

For a domain with a central cell of maximum microcline ($\Gamma=0.04$), and for which $M/L=0.12$ (Table 1), $E_s=1.5\times10^{-20}J$ per unit cell.

Inversion Energy

Implicit in this discussion and analysis of strain is the assumption that the strain energy is provided by the energy released as orthoclase transforms to microcline. Such an assumption can be tested using thermodynamic data to evaluate the lattice energy released during ordering and comparing this with the strain energy.

The heat of inversion of sanidine to microcline, ΔH, is *2.0* Kcal/mole (Waldbaum and Robie 1971), or 5.5×10^{-20} *J*/unit cell. There are no data for the heat of conversion of orthoclase to microcline, but an estimate can be made from an order indicator such as Δbc. K-feldspar begins to show triclinic character between $\Delta bc=0.8$ and *0.9* (Stewart and Wright 1974); Δbc for the Kameruka monoclinic feldspars ranges up to *0.89*, with a concentration of values at *0.85*, whereas Δbc for triclinic specimens ranges down to *0.83*. If it is assumed that Δbc is a linear indicator of order, and also of ΔH between any two states, then ΔH for the transition orthoclase-microcline is: $(1-0.85)/(1-0.5)\,\Delta H$ (san-mic)$=1.65\times10^{-20}$ *J*/unit cell. There is therefore exactly enough energy released by ordering to produce the observed strain.

Considering the assumptions used for the strain analysis the closeness of the agreement between these two values may be partly fortuitous. The general agreement is not. The dominant terms in the expression for strain energy are those involving C_{66} (representing the pure shear component between x and y) and the term involving C_{11}, the component of compressive strain parallel to *OX*. It is in these factors that the model is most firmly based on the observational evidence. The introduction of chevron character to the domains reduces *Es*, (a similar strain analysis gives $Es=0.75\times10^{-20}$ *J*/unit cell in a pure chevron domain), but this reduction is offset by an (unknown) increase in internal energy due to twinning. It seems

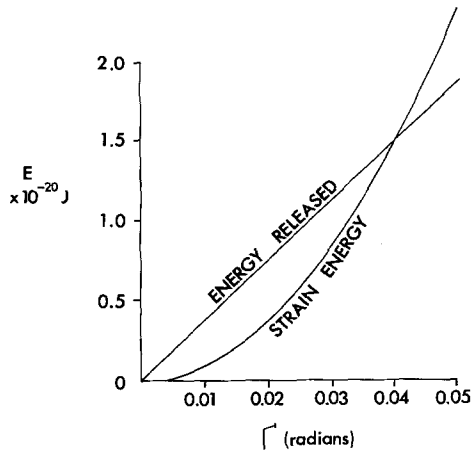

Fig. 9. Diagrammatic representation of a linear release of energy, E, with ordering, and a parabolic increase of strain energy with changing $\Gamma(=\pi(90-\gamma)/180)$

unlikely that a part chevron part sinusoidal domain would have an internal strain plus twin energy much less than $1.5.10^{-20}$ J per unit cell.

Discussion

This strain analysis suggests that the build-up of strain retards the ordering of triclinic K-feldspars. From Stewart and Ribbe's (1969) analysis of ordering, and from the structural analyses of microclines (Brown and Bailey 1964; Bailey 1969; Ribbe 1979), the Al content of Tl sites for unstrained microcline is continuous and linear between $\Delta bc \simeq 0.85$, $\Delta\alpha^*\gamma^* = 0$ and $\Delta bc = 1.0$, $\Delta\alpha^*\gamma^* = 1.0$. Thus, ideally, $\Delta\alpha^*\gamma^*$ (and consequently Γ) is a linear function of energy release during ordering. On the other hand, the strain energy increases as Γ^2, so that when Γ becomes large enough (when enough unit cells in a domain have ordered) the energy advantage in ordering is offset by the build-up of strain energy (Fig. 9) and ordering slows.

The magnitude of the strain is also dependent on domain width. Provided $M << L$, N, the major term in the expression for E_s is the constant 8.8. The dependence of E_s on M^2/L^2, though a direct consequence of the model, shows that if the domains become too wide it is energetically better for the domain to twin than to continue widening. Indeed, the total internal energy of strained, twinned microcline will be greater than that calculated here, because no account has been taken of the internal energy difference between twinned and untwinned feldspar. Each twin plane must increase the internal energy by a finite amount, relative to an untwinned crystal; otherwise the stable maximum microcline structure would be one of alternating left- and right-handed unit cells. In our sinusoidal model there is minimum angular change across the twin boundaries, and probably minimum twin boundary energy. We therefore conclude that, in the absence of an external energy source, a balance between energy released by ordering and energy used in domain formation is reached at a value of $\Gamma < 0.04$ for the Kameruka feldspars. The metastable persistence of orthoclase in plutonic rocks may well be explained by the strain retardation of inversion.

Addition of energy to a K-feldspar that has reached the dimpled terrane stage of Al/Si ordering may allow the accumulated strain to be released by dislocation movement. In the case of the Kameruka feldspars, tectonic faulting appears to have provided the impetus to rearrange the structure into maximum microcline geometry. The bimodal distribution of triclinicities found for these feldspars can now be explained as representing strained and unstrained crystals, and the discontinuity in $\Delta\alpha^*\gamma^*$ represents the effects of release of strain energy by shear.

Summary

1. The inversion of orthoclase (monoclinic) to microcline (triclinic) in the absence of external stress, produces a structure composed of alternately left- and right-handed albite-twin related domains, in which α and γ vary approximately sinusoidally. The domains are tabular on (010); their widths are less than one tenth their other dimensions;

2. Analysis of domain size and character and of lattice strain shows that the energy released by Al/Si ordering is balanced by the strain energy developed when triclinic domains are restricted to a monoclinic shape;

3. The X-ray measured cell angles are an average over the domain, and are significantly closer to monoclinic values than the angles of unstrained microcline with the same degree of Al/Si order;

4. A bimodal distribution of triclinicities for the Kameruka K-feldspar megacrysts results from measurements made on two different populations of triclinic crystals: strained, domain-structured intermediate microcline, and sheared, strain-released maximum microcline.

Conclusion

From these observations we conclude that triclinicity is not necessarily directly proportional to the degree of Al/Si ordering in the feldspar, and that considerable caution should be used when drawing geological

conclusions from triclinicity determinations. The build-up of strain in the microcline lattice is seen to act as a barrier to the development of triclinic geometry. The result is that the feldspar does not order past a certain stage, the stage at which the release of energy with order balances the strain energy. The particular balance reached depends on the situation of the feldspar, and if the strain can be released, whether by shearing, hydrothermal activity, or another process, ordering can proceed unhindered; thus, the measured triclinicity of a K-feldspar may represent the temperature of the final strain-releasing process.

Acknowledgements. This work was supported in part by grants EAR 77-00128 and 79-26375 from the Earth Sciences Division of the National Science Foundation. RAE particularly thanks Professor Dr. W. Wimmenauer and Dr. J. Keller for the use of facilities at the Mineralogisches Institut, Universität Freiburg, during the analysis of the data. Drs. J.N. Boland and G.E. Brown gave useful criticism of early drafts of the paper.

References

Bailey SW (1969) Refinement of an intermediate microcline structure. Am Mineral 54:1540–1545

Brown BE, Bailey SW (1964) The structure of maximum microcline. Acta Crystallogr 17:1391–1400

Eggleton RA (1979) The ordering path for igneous K-feldspar megacrysts. Am Mineral 64:906–911

Goldsmith JR, Laves F (1954a) The microcline sanidine stability relations. Geochim Cosmochim Acta 5:1–19

Goldsmith JR, Laves F (1954b) Potassium feldspars structurally intermediate between microcline and sanidine. Geochim Cosmochim Acta 6:100–118

McConnell JDC (1971) Electron optical study of phase transformations. Mineral Mag 38:1–120

McLaren AC (1978) Defects and microstructures in feldspars. Chemical Physics of solids and their surfaces. Chem Soc 7:1–30

Martin RF (1974) Controls of ordering and subsolidus phase relations in the alkali feldspars. In: The Feldspars. NATO advanced study Institute, Manchester Univ Press

Nye JF (1972) Physical properties of crystals: their representation by tensors and matrices. Oxford, Clarendon Press

Ribbe PH (1979) The structure of a strained intermediate microcline in cryptoperthitic association with twinned plagioclase. Am Mineral 64:402–408

Rhyzhova TV, Aleksandrov KS (1965) The elastic properties of potassium-sodium feldspars. Isvest Akad Nauk SSSR. Physics of the solid earth, pp 53–56 (Engl transl)

Stewart DB, Ribbe PH (1969) Structural explanation for variations in cell parameters of alkali feldspar with Al/Si ordering. AJS 267A:444–462

Stewart DB, Wright TL (1974) Al/Si order and symmetry of natural alkali feldspars, and the relationship of strained cell parameters to bulk composition. Bull Soc Fr Mineral Cristallogr 97:356–377

Smith JV (1974) Feldspar Minerals. Springer Verlag, Berlin

Veblen DR, Buseck PR (1979) Chain width order and disorder in biopyriboles. Am Mineral 64:687–700

Waldbaum DR, Robie RA (1971) Calorimetric investigation of Na-K mixing and polymorphism in the alkali feldspars. Z Kristallogr Mineral 134:381–420

Wright TL, Stewart DB (1968) X-ray and optical study of alkali feldspars: I. Determination of composition and structural state from refined unit-cell parameters and 2V. Am Mineral 53:38–87

Received April 28, 1980; Accepted August 11, 1980